Review

Non-aqueous Sol-Gel Routes to Metal Oxide Nanocrystals under Solvothermal Conditions: Review and Case Study on Doped Group IV Metal Oxides

Andrea Pucci[a] and Nicola Pinna[a, b]

[a] Department of Chemistry, CICECO, University of Aveiro, 3810-193 Aveiro, Portugal
[b] World Class University (WCU) program of Chemical Convergence for Energy & Environment (C2E2), School of Chemical and Biological Engineering, College of Engineering, Seoul National University (SNU), Seoul 151-744, Korea

Reprint requests to Prof. N. Pinna. E-mail: pinna@ua.pt or pinna@snu.ac.kr

Z. Naturforsch. **2010**, *65b,* 1015 – 1023; received March 12, 2010

Over the last decade, the number of publications concerning the non-aqueous sol-gel synthesis of metal oxide nanostructures has rapidly increased, as this method affords an immense variety of sizes and shapes of the products. This review highlights the versatility of non-aqueous sol-gel routes, under solvothermal conditions, to metal oxide and hybrid materials. In particular, the easier control over the reaction kinetics, compared to aqueous methods, allows to better match the reactivity between metal oxide precursors. This permits to produce complex multimetal and doped oxides at low temperature, as it is discussed in detail for the case of doped group IV metal oxides.

Key words: Metal Oxides, Nanocrystals, Sol-Gel Process, Solvothermal Synthesis

Introduction

The fundamental and applied scientific importance of nanomaterials has, without any doubt, been demonstrated in the last decade. The peculiar conductive, magnetic, optical, and chemical properties at the nanoscale led to several breakthroughs in various fields. Biomedical applications, long-life batteries, spintronic devices, and solar cells are just a few examples of how these nanomaterials can be exploited [1]. As the knowledge and development of nanoscience advances, a growing attention is given to the development of versatile, cheap and scalable synthesis methods allowing at the same time the precise control of the composition, the size and the shape at the nanometer scale. As a matter of fact, the above mentioned properties are strongly affected by the size and shape of the nanostructures. The traditional path to inorganic materials is the ceramic approach; high temperature is used to provide interdiffusion of metal ions between intimately mixed solid precursors. On the one hand, this method is universally applicable and leads to high-density materials and a high degree of crystallinity. On the other hand, it does not permit the control of the shape, size and size distribution at the nanometer scale. Moreover, the major limitation is the thermodynamic control over the reaction, leading only to the more stable compounds. Many wet chemistry methods have been developed to achieve the preparation of other interesting materials (*i. e.* kinetically promoted and metastable phases). Among these protocols, the solvothermal method plays an outstanding role. Solvothermal synthesis generally refers to a reaction occurring in the presence of any kind of solvent in a sealed system (*e. g.* in an autoclave) with the temperature raised above the boiling point of the solvent. In this review, we concentrate on non-aqueous syntheses focusing on metal oxide nanocrystals.

Solvothermal Synthesis

The understanding of the formation mechanism and the growth of nanocrystals in solution in order to direct the synthesis towards the desired product is one of the major objectives of nanochemistry. This would make solution approaches more suitable for applications, but also allow cheaper and greener paths. Up to now, it is nearly impossible to foresee the morphology of nanoparticles, and the tailoring of their composition, size and shape can be done only

0932–0776 / 10 / 0800–1015 $ 06.00

on an empirical basis [2]. To attain this objective, the comprehension of the reaction mechanisms is clearly the starting point [3, 4]. The solvothermal method is particularly suitable from this point of view as the reaction systems are relatively simple, especially when no surfactants or capping agents are used. The study of organic byproducts allows the investigation of how the precursors interact, suggesting a way to set the different reaction parameters. [3]. The most common reactions occurring in non-hydrolytic solvothermal synthesis are thermolysis and metathesis reactions. Other routes have been exploited which go through a complex-formation process or a reduction/oxidation as in the case of γ-LiV_2O_5 nanorods [5].

Thermolysis

The formation of nanomaterials by thermal decomposition of metal complexes has been mainly applied to obtain metals. The decomposition of the ligands generally involves alkene elimination and the formation of a hydroxyl group. One of the first attempts for the synthesis of metal oxides were made by Inoue and coworkers [6]. Their synthesis approach involved the thermal decomposition of metal complexes, at temperatures ranging from 200 to 300 °C, in diverse glycols, ethylene glycol and 1,4-butanediol being the most investigated. Through this route several metal oxides [7 – 9] and phosphates [10] were synthesized. Simple alcohols have also been exploited. For example, Inoue compared the products obtained reacting aluminum alkoxides in various solvents under solvothermal conditions [11]. Simple primary alcohols led to hybrid materials in which solvent alcohol molecules are incorporated between boehmite layers through covalent bonding [12]. Similar results were obtained in glycol media but, in these cases, the organic moieties in the derivate of boehmite, presenting two functional groups, act as bridges between the inorganic layers [13]. The length of the carbon chain affects the size of the final product. Thus, these approaches allow the synthesis of hybrid materials with tunable size and interlayer distance. Noteworthy, the alkoxide (glycoxide) derivatives of boehmite can eventually be an intermediate step toward the synthesis of γ-alumina by increasing time, temperature or concentration of the precursor during the reaction [11, 14]. Other more complex solvents were used, such as 2-methoxyethanol, leading to the oxides of cerium [15], gallium [16] or rare earth metals (*RE*) [17]. Metal hydroxides were also prepared reacting $RE(NO_3)_3$ in alcohols or glycols at 250 °C, obtaining different morphologies [18]; only after calcination the pure oxides were obtained. Recently, Julian-Lopez *et al.* synthesized a mesoporous $Er_2Ti_2O_7$ pyrochlore structure in ethanol at 170 °C, however, very probably, the reaction mechanism is more complex than a simple thermal decomposition in this case [19].

Metathesis

Some advantages such as the cheapness of the solvothermal approach towards other synthesis methods are even more pronounced in the case of metathesis reactions, where it is not necessary to reach the thermal decomposition of the precursor, and lower temperatures are often allowed. Three polymorphs of titania, namely anatase, rutile and brookite, were obtained from $TiCl_4$ under solvothermal condition (110 °C) just varying the solvent (diethyl ether, ethanol and *tert*-butanol, respectively) [20]. Other examples of materials which were prepared through a metathesis approach are hollow spheres of hematite [21] or tetragonal CoO [22] in ethanol and in the presence of a surfactant.

Alkylhalide, ether, ester or amide eliminations, and C–C bond cleavage or formation processes, are some of the processes taking place during metal oxide formation. Since they have already been reviewed elsewhere, they will not be further discussed here [3, 4, 23 – 25]. Most of these synthesis paths are exploited for the formation of metal oxide nanostructures through the "benzyl alcohol route".

The "Benzyl Alcohol Route"

From a general point of view, this non-aqueous and/or non-hydrolytic sol-gel method allows the synthesis of nanoparticles even in sub-solvothermal conditions (typically between 40 and 180 °C) exploiting metal halides as precursors. Several oxides have been obtained through this approach [26 – 28]. Nevertheless, it is difficult to avoid the presence of halide impurities in the final product making this path not suitable when high purity is required. In such cases, by exploiting the advantages of solvothermal syntheses involving slightly higher temperatures (the boiling point of benzyl alcohol is 205 °C), it is possible to transform metal complexes into the respective oxides.

The reaction of a metal alkoxide in benzyl alcohol to form M–O–M bonds often occurs through ether elimination, as in the cases of TiO_2, ZrO_2, HfO_2, Nb_2O_5,

and SnO_2 [29 – 33]. Other more stable and/or less expensive metal precursors such as carboxylates can also be used. Their solvothermal treatment in benzyl alcohol leads to the elimination of the corresponding ester. As a typical example, benzyl acetate was found in the reaction mixture after the production of zinc oxide both by conventional heating [34, 35] and under microwave irradiation [35, 36]. The ester elimination pathway is well known in zinc carboxylate-alcohol systems [3] and has been observed in different cases [37, 38]. Unfortunately, the processes involved in the reactions were not studied systematically for all the nanostructures produced using this approach. No mechanisms have been proposed for the synthesis of manganese oxides [39], while a path can be guessed in the case of iron oxides. Several precursors were investigated for the synthesis of either magnetite or maghemite nanoparticles [35, 40]. An ester elimination mechanism was claimed by Gotic and Music [41] in the case of iron acetate reacting in ethanol or octanol. However, when iron acetylacetonate is reacted in benzyl alcohol or benzylamine the formation of Fe–O–Fe bridges follows a mechanism involving the cleavage of a C–C bond in the acetylacetonate moiety [4, 42]. In the case of benzylamine, the C–C bond cleavage leads to iron-enolate species which further react with the solvent molecules promoting ketimine condensation. This last reaction leads to species presenting hydroxyl groups that can further condensate to iron oxide nanoparticles [42].

It is important to mention that the metal center often acts as a catalyst leading to the formation of new carbon-carbon links. During the synthesis of CeO_2 nanoparticles from $Ce(OiPr)_3$ 4-phenyl-2-butanol and 1,5-diphenyl-3-pentanol were found in the reaction mixture [43, 44]. The side products are suggested to be due to a coupling activated by the formal deprotonation of a methyl group of the isopropoxide ligand. A similar coupling occurs also during the formation of alkaline earth metal titanates [45, 46]. A nucleophilic attack of a β-carbon atom of the titanium isopropoxide precursor at an activated benzyl alcohol group occurs. Ba or Sr ions catalyze the reaction stabilizing a benzylate which initiates the process by deprotonating the methyl group in β-position. Other interesting perovskites or ternary oxides have been synthesized through the benzyl alcohol route: $BaZrO_3$ [46], $LnNbO_4$ [47, 48], $YNbO_4$ [48], $LiNbO_3$ [46], $MnNb_2O_6$ [48], $NaNbO_3$ [49], $NaTaO_3$ [49], tin-doped indium oxide (indium tin oxide, ITO) [50, 51], and $La_{1-x}A_xMnO_3$ (A = Ca, Sr, or Ba [52]). The possibility of matching the different reactivity of diverse kinds of metal complexes in benzyl alcohol makes this approach extremely versatile even for the preparation of complex materials [53].

Another possibility offered by this synthetic path is the formation of nanostructured hybrid materials. The benzyl alcohol (or in some cases a derivative resulting from the process) acts as a capping ligand to specific crystallographic facets of the *in situ*-formed inorganic nanocrystals allowing to obtain highly anisotropic shapes. Simultaneously, it stabilizes and phase-separates the inorganic nanocrystals by creating a highly ordered superstructure with spatially well-defined domains [54]. The combination of organic and inorganic components leads to multifunctional materials with properties arising from the two constituents but also from the interface between them [55]. The first hybrid materials synthesized in benzyl alcohol were Y_2O_3-based nanostructures [56]. The reaction of $Y(OiPr)_3$ in benzyl alcohol at 250 °C led to a lamellar structure in which benzoate molecules were arranged in between the inorganic layers. Following these results, the approach was extended to rare earth oxide nanohybrids such as gadolinium, neodymium, erbium and samarium oxides [57, 58].

Another family of hybrid materials was recently obtained mixing alkaline earth metal oxide precursors (Ca, Ba or Sr) and aluminum isopropoxide at 275 °C.

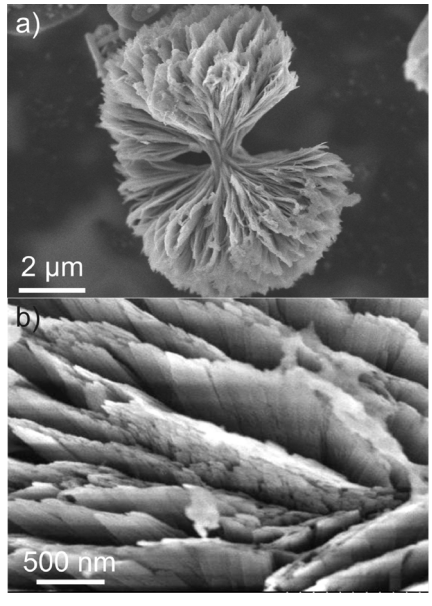

Fig. 1. TEM images of a single particle $CaAl_4O_7$ (a) and detail of the surface region (b).

The synthesis led to flower-like spherical particles consisting of generally uniform thin platelets or needles stabilized by benzoate ligands (Fig. 1) [59].

When tungsten chloride is reacted in anhydrous benzyl alcohol pure inorganic platelets of tungstite are obtained [26, 60]. A small quantity of a specific ligand, introduced during the synthesis, dramatically affects the morphology and the supramolecular arrangement of the final material. For example, with deferoxamine mesylate the final material is constituted of bundles of long wires of $W_{18}O_{49}$ which have a uniform diameter of about 1.3 nm and an aspect ratio of more than 500. They are kept together by π-π interactions between benzaldehyde molecules adsorbed at their surface [60]. Similar nanowires were also obtained without additional ligands when tungsten isopropoxide was used instead of tungsten chloride [61]. When 4-*tert*-butylcatechol was used as ligand, long rods consisting of highly ordered lamellar organic-inorganic hybrid structures similar to the ones found for the rare earth hybrid materials were observed [62].

From these examples it is clear that different precursors lead to different nanostructures, but in these systems, the addition of an inert solvent plays also a crucial role in determining shape, size and polydispersity. As a typical example, the synthesis of Co-doped ZnO in benzyl alcohol results in a heterogeneous sample where nanoparticles and nanorods coexist, showing a quite large size distribution (Fig. 2) [34]. If under the same reaction conditions benzyl alcohol is partly replaced by anisole acting as an inert solvent, short rods are formed. Finally, well defined nanowires are obtained when the benzyl alcohol content was further decreased (just traces).

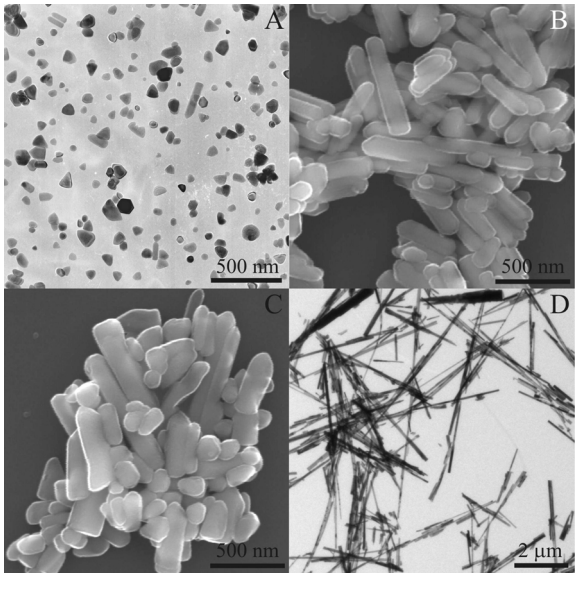

Fig. 2. TEM images of Mn-doped ZnO in pure benzyl alcohol (A), and of Co-doped ZnO in anisole with traces of benzyl alcohol (D). SEM images of pure (B) and Co-doped (C) ZnO synthesized in benzyl alcohol/anisole (5/95).

Benzyl alcohol was also used as solvent for the synthesis of metal phosphate nanocrystals and hybrid materials. Willinger *et al.* synthesized nanocrystalline titanium, zirconium, vanadium, yttrium, and lanthanide phosphates at yields above 90 % from metal chlorides and/or alkoxides in benzyl alcohol in the presence of anhydrous phosphoric acid [63]. The synthesized lanthanide phosphates show high emission efficiencies when doped with terbium, proving the good crystalline quality of the as-synthesized nanocrystals. Bilecka *et al.* [64] and Yang *et al.* [65] synthesized $LiFePO_4$ for application in Li ion batteries. Finally, Di *et al.* showed that the approach can also be used to produce highly luminescent rare earth phosphonate hybrid nanostructures [66].

The reducing power of the benzyl alcohol seems to be the main limitation of the versatility of the approach. Cations sensitive towards reduction to the respective metals cannot be used. A typical example is the attempted synthesis of lead oxide or titanate, where lead is reduced to Pb^0. In these cases alternative non-reductive solvents, such as ketones, can be used [67].

A Case Study: Doped Group IV Metal Oxides

Titania, zirconia and hafnia have attracted interest due to their wide range of applications. These materials were also prepared through the benzyl alcohol route [2]. In this section we review the doping behavior of group IV oxides with different transition metal and lanthanide ions. It has recently been shown that the "benzyl alcohol route" allows not only the production of good quality group IV oxide nanocrystals in their more interesting metastable phases, but offers also the possibility to tailor their properties by a homogeneous and controlled addition of dopants.

Fe- and Co-doped titania

Titania nanocrystals have been among the most investigated, especially for their high photocatalytic capacity [68]. The doping has proven to enhance the efficiency with respect to reduction and oxidation reactions [69]. Furthermore, TiO_2 was proposed as a pos-

sible high-T_C diluted magnetic semiconductor material when doped with transition metal ions [70, 71]. Djerdj and coworkers carried out an interesting study on Fe- or Co-doped titania [72], investigating the influence of the solvent (*i. e.* benzyl alcohol, butanone or an isovolumetric mixture of them) on the synthesized nanoparticles. They also focused their attention on different titanium precursors (titanium tetrachloride and titanium tetraisopropoxide) but maintaining a fixed load of the dopant (3 %).

In all the studied samples the nanoparticles showed a high degree of crystallinity of the tetragonal TiO_2 anatase modification (Fig. 3). The morphology of the powder was observed by a combination of XRD, TEM and related techniques. Different from the undoped nanocrystals, which are spherical, the doped TiO_2 nanocrystals show a faceted octagonal bipyramidal shape. On the one hand, the use of the alcohol rather than the ketone leads to a lower tendency to form agglomerates and to slightly larger nanoparticles. For example, the Fe-doped particles obtained using Ti(O*i*Pr)$_4$ are around 7.4 nm in diameter when synthesized in benzyl alcohol, compared to 6.8 nm in butanone. On the other hand, the titanium precursor is the factor that affects the final product most. The mean diameter decreases from 14 to 8.5 nm using the alkoxide instead of the halide. Moreover, using $TiCl_4$ leads to a particle size distribution twice as large.

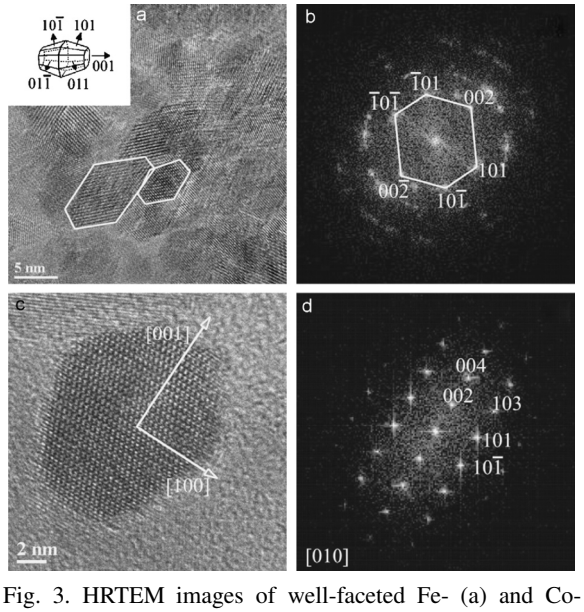

Fig. 3. HRTEM images of well-faceted Fe- (a) and Co-doped (c) TiO_2 and their powder spectra (b and d). Reproduced with permission from ref. [72].

The doping efficiency is also affected by the nature of the Ti precursor. The ratio Ti/transition metal was evaluated by EDX on Co-doped TiO_2 (synthesized from Ti(O*i*Pr)$_4$ and $CoAc_2$), and it was found to be only 1.1 % compared to the expected 3 %. The EDX spectra of the Fe-doped samples showed no evidence of Fe. Considering the brownish color of the powder and the absence of clustering from XRD and TEM analyses, it is clear that the effective percentage of iron solubilized in the titania matrix must be below the resolution of the instrument. A rough idea of the doping concentrations came from magnetic measurements. All the studied samples displayed a paramagnetic behavior, matching the Curie-Weiss law. Assuming that the dopants did not undergo redox reactions and that the entire magnetic response is due to Co or Fe, it is possible to extrapolate the values from the susceptibility curves. The as-calculated value for Fe-doped titania is 0.22 % only, which is in agreement with the previous conjecture. In the case of cobalt the values are 0.7 and 0.02 for nanoparticles synthesized from Ti(O*i*Pr)$_4$ and $TiCl_4$, respectively.

Eu-, Mn- and Cr-doped zirconia

Due to the diverse applications of zirconia in catalysis, oxygen sensors, ceramics, and fuel cells [73 – 77], several studies have been carried out on the synthesis of the cubic fluorite-type zirconia, which is the more suitable among the three polymorphs of ZrO_2. Unfortunately, the transformation between the modifications is reversible and, thus, the cubic phase can only be obtained by adding another cation or by a size effect [78]. Doping with Y, Mg, Ce, Ca, Cr, and Si has been exploited for this purpose in the bulk, while on the nanometric scale it is the inherent surface energy of the nanoparticles which leads to stabilization. The synthesis of undoped zirconia through the benzyl alcohol route leads to particles of 3 – 4 nm with a cubic modification as it has recently been shown [30, 31]. Nevertheless, the doping of such a material is very appealing to induce optical or magnetic properties. Recently, the substitution of lanthanides and transition metals in zirconia, through the benzyl alcohol route, has been proved by two groups [79 – 81]. The doping with those ions, up to 15 %, does not destabilize the cubic modification and preserves the morphology: the particles exhibit in all cases a spherical shape with a narrow size distribution around 3 – 4 nm.

Ninjabadgar *et al.* [79] studied Eu-doped zirconia aiming at an efficient photosensitive material. Due to

the high refractive index of the matrix, Eu-coated or -doped zirconium dioxide systems have already been investigated [82 – 85]. The dopant environment and the zirconia modification play a decisive role for the final properties of the material. The red light emitted by Eu^{3+} ions is mainly due to an intense band at 613 nm, corresponding to the electric dipole transition ($^5D_0 \rightarrow {}^7F_2$). The magnitude of the emission and the inhomogeneous broadness of the peaks suggest a variety of local chemical environments, ranging between sevenfold and sixfold symmetries [86, 87]. Observation of the photoluminescence decay behavior on the emission line shows the presence of two contributions. The signal can be attributed to dopant ions either on the surface or in the core of the nanoparticles. The drop of the lifetime with the increase of the concentration proves the homogeneity of the doping, as it is due to the formation of Eu–Eu bonds leading to a non-radiative dispersion of the excitation.

The study of the surroundings of the dopant ions is even more important for the understanding of the magnetic properties in the case of transition metal-doped systems. The occurrence of clusters or segregations of the magnetic centers is really difficult to detect on such a small scale, but it may strongly affect the magnetic behavior. For this reason, several techniques (*i. e.* XRD, UV/Vis, EPR, ICP-AES, TEM, EELS, EDX) have been used by Clavel, Pucci and coworkers [80, 81] to rule out the presence of secondary phases in manganese- or chromium-doped nanoparticles. For this aim, one of the most proper analyses is the electron paramagnetic resonance technique (EPR), as the signal resulting from the unpaired electrons of the dopant ion is perturbed by the nature and the position of near neighbor nuclei. Although Mn^{3+} and Cr^{4+} ions are often silent, plenty of information can be gained probing doped matrices concerning the oxidation state, the local environment and the spin coupling of the dopand. The insertion of manganese into the zirconia structure results in a valence state between II and III [80]. The EPR spectra of those samples show a broad band due to the magnetic interactions of the Mn ions superimposed by hyperfine splitting resulting from isolated ions. By applying thermal treatment on the system it is possible to monitor the segregation of the magnetic ions. The electron resonance of samples annealed above 600 °C under an oxygen atmosphere displays a progressive vanishing of the sextuplet and a decrease in intensity most probably due to the formation of manganese oxide clusters and to the recrystallization of the zirconia matrix in the tetragonal modification. The clustering is further confirmed by magnetic measurements: the pristine products show a paramagnetic behavior whereas the annealed samples are ferrimagnetic. The ZFC/FC curves show the appearance of a maximum at 42 K which matches the values reported in the literature for Mn_3O_4 in diluted systems.

Cr-doped zirconia nanoparticles analyzed by EPR show only a very weak peak at g = 5.33 resulting from Cr^{3+} ions homogenously dispersed in the matrix. Since all chemical characterizations clearly prove an effective doping, EPR could indicate the presence of Cr^{4+} in an octahedral environment and a mean oxidation state between III and IV. This assumption has been confirmed by studying the magnetic properties. The Langevin fit of the hysteresis loops gives estimated values above 2 μ_B/Cr (*e. g.* 2.32 μ_B/Cr for $Zr_{0.980}Cr_{0.020}O_2$) which are consistent with the suggested mixed valence. Interestingly, any pristine paramagnetic doped nanoparticles turn ferromagnetic after calcination at 650 °C (Fig. 4). In this case the mag-

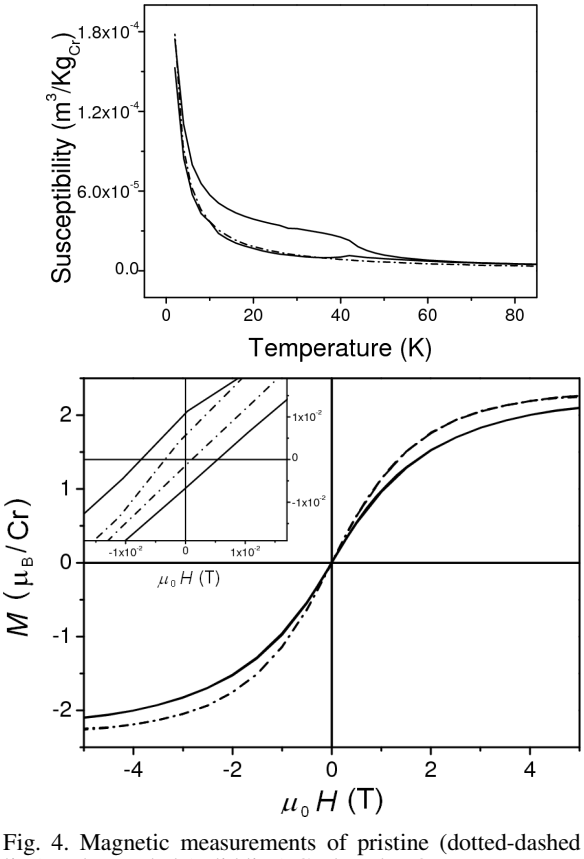

Fig. 4. Magnetic measurements of pristine (dotted-dashed line) and annealed (solid line) Cr-doped ZrO_2.

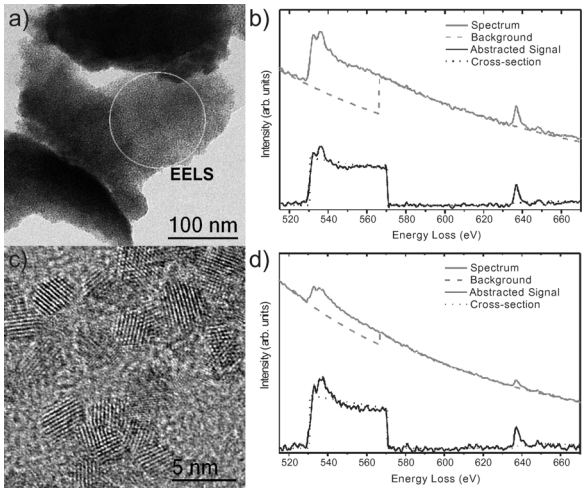

Fig. 5. TEM images (a, c) and corresponding EELS spectra (b, d) of Mn-doped HfO_2.

netic behavior cannot be assigned to segregation of the dopant as the Curie temperature of 43 K is not ascribable to any kind of known chromium oxide system. The intrinsic ferromagnetism rises after the oxidation of a certain amount of Cr ions due to the annealing under oxygen. Indeed, for the calcined samples a very intense and narrow peak is observable in the EPR spectra at $g = 1.97$ which most probably is to be attributed to Cr^{5+} ions on the surface of the nanoparticles.

Mn- and Cr-doped hafnia

As an effect of the lanthanide contraction, zirconium and hafnium have similar ionic radii (72 and 71 pm, respectively). Presenting also an equivalent arrangement of the electrons, the two metals have similar physical and chemical properties. Nonetheless, the stability of the polymorphs is different. Unlike zirconia nanoparticles, for hafnia the cubic phase is not stabilized by the nanometric size. Undoped hafnia nanoparticles are in the thermodynamically stable monoclinic phase with an ellipsoidal morphology [29]. Doping with chromium (up to the maximum effective concentration of 7 %) does not lead to a different modification [81]. On the other hand, manganese ions substituted into the structure tend to stabilize the cubic phase. The addition of more than 3 % of the Mn precursor to the reaction directs the crystal growth to form a cubic system. This transition modifies also the shape of the nanoparticles from ellipsoidal to faceted pseudospherical, while no sensible variation in size is observed (Fig. 5). Noteworthy, the doping behavior in the case of manganese is similar to the Mn-doped zirconia system whereas in the case of chromium the monoclinic structure of hafnia seems to host ions with a higher mean oxidation state. Indeed, the δ signal at $g = 5.33$ due to Cr^{3+} is not visible in the EPR spectra. The lack of the intense β signal commonly assigned to Cr_2O_3 clusters is a further proof of the absence of segregation in these systems.

Conclusion

In this article the versatility of non-aqueous sol-gel chemistry, under solvothermal conditions, for the synthesis of metal oxide nanostructures has been discussed [4]. Particular emphasis was put on the case of doped metal oxides in order to highlight one of the most promising advantages of these chemical routes. That is, possibilities are explored to more easily match the reactivity of the metal complexes and of the dopants compared to aqueous systems. As a matter of fact, some of the materials discussed were up to now only accessible by high-temperature solid-state reactions. Finally, the relatively recent application of the microwave technique proved to dramatically increase the kinetic of the processes allowing faster and greener reactions [88]. These findings will clearly help to increase the popularity of non-aqueous sol-gel approaches to complex metal oxide nanocrystals.

Acknowledgements

This work was partially supported by the WCU (World Class University) program through the National Research Foundation of Korea funded by the Ministry of Education, Science and Technology (R31-10013) and FCT projects (PTDC/CTM/65667/2006) and (PTDC/CTM/098361/2008). A. Pucci is grateful for the supports of FCT (grant No. SFRH/BD/45177/2008). The authors thank Dr. G. Clavel for fruitful discussions.

[1] A. P. Alivisatos, *J. Phys. Chem.* **1996**, *100*, 13226.
[2] N. Pinna, M. Niederberger, *Angew. Chem.* **2008**, *120*, 5372; *Angew. Chem. Int. Ed.* **2008**, *47*, 5292.
[3] M. Niederberger, G. Garnweitner, *Chem. Eur. J.* **2006**, *12*, 7282.
[4] M. Niederberger, N. Pinna, *Metal Oxide Nanoparticles in Organic Solvents*, Springer, London, **2009**.

[5] Y. W. Wang, H. Y. Xu, H. Wang, Y. C. Zhang, Z. Q. Song, H. Yan, C. R. Wan, *Solid State Ionics* **2004**, *167*, 419.
[6] M. Inoue, H. Tanino, Y. Kondo, T. Inui, *J. Am. Ceram. Soc.* **1989**, *72*, 352.
[7] M. Inoue, H. Kominami, T. Inui, *Research on Chemical Intermediates* **1998**, *24*, 571.
[8] K. Kubo, S. Hosokawa, S. Furukawa, S. Iwamoto, M. Inoue, *J. Mater. Sci.* **2008**, *43*, 2198.
[9] S. Iwamoto, K. Saito, M. Inoue, K. Kagawa, *Nano Letters* **2001**, *1*, 417.
[10] T. Nakamura, T. Inui, M. Inoue, T. Miyake, *J. Mater. Sci.* **2006**, *41*, 4335.
[11] M. Inoue, *J. Phys. Condens. Matter* **2004**, *16*, S1291.
[12] M. Inoue, M. Kimura, T. Inui, *Chem. Mater.* **1999**, *12*, 55.
[13] M. Inoue, H. Kominami, T. Inui, *J. Chem. Soc., Dalton Trans.* **1991**, 3331.
[14] K. Pansanga, O. Mekasuwandumrong, J. Panpranot, P. Praserthdam, *Kor. J. Chem. Eng.* **2007**, *24*, 397.
[15] M. Inoue, M. Kimura, T. Inui, *Chem. Commun.* **1999**, 957.
[16] S.-W. Kim, S. Iwamoto, M. Inoue, *Ceram. Int.* **2009**, *35*, 1603.
[17] T. Kobayashi, S. Hosokawa, S. Iwamoto, M. Inoue, *J. Am. Ceram. Soc.* **2006**, *89*, 1205.
[18] S. Yin, S. Akita, M. Shinozaki, R. Li, T. Sato, *J. Mater. Sci.* **2008**, *43*, 2234.
[19] B. Julián-López, M. Martos, N. Ulldemolins, J. Odriozola, A. E. Cordoncillo, P. Escribano, *Chem. Eur. J.* **2009**, *15*, 12426.
[20] P. Arnal, R. J. P. Corriu, D. Leclercq, P. H. Mutin, A. Vioux, *J. Mater. Chem.* **1996**, *6*, 1925.
[21] S. Lian, E. Wang, L. Gao, D. Wu, Y. Song, L. Xu, *Mater. Res. Bull.* **2006**, *41*, 1192.
[22] Y. Ye, F. Yuan, S. Li, *Mater. Lett.* **2006**, *60*, 3175.
[23] G. Garnweitner, M. Niederberger, *J. Mater. Chem.* **2008**, *18*, 1171.
[24] A. Vioux, *Chem. Mater.* **1997**, *9*, 2292.
[25] P. H. Mutin, A. Vioux, *Chem. Mater.* **2009**, *21*, 582.
[26] M. Niederberger, M. H. Bartl, G. D. Stucky, *J. Am. Chem. Soc.* **2002**, *124*, 13642.
[27] M. Niederberger, M. Antonietti, in *Nanomaterial Chemistry: Recent Developments and New Directions*, (Eds.: C. N. R. Rao, A. Müller, A. K. Cheetham), Wiley-VCH, Weinheim, **2007**, pp. 119.
[28] J. Ba, J. Polleux, M. Antonietti, M. Niederberger, *Adv. Mater.* **2005**, *17*, 2509.
[29] N. Pinna, G. Garnweitner, M. Antonietti, M. Niederberger, *Adv. Mater.* **2004**, *16*, 2196.
[30] S. Zhou, G. Garnweitner, M. Niederberger, M. Antonietti, *Langmuir* **2007**, *23*, 9178.
[31] G. Garnweitner, L. Goldenberg, O. Sakhno, M. Antonietti, M. Niederberger, J. Stumpe, *Small* **2007**, *3*, 1626.
[32] N. Pinna, M. Antonietti, M. Niederberger, *Colloids Surf. A* **2004**, *250*, 211.
[33] N. Pinna, G. Neri, M. Antonietti, M. Niederberger, *Angew. Chem.* **2004**, *116*, 4445; *Angew. Chem. Int. Ed.* **2004**, *43*, 4345.
[34] G. Clavel, M. G. Willinger, D. Zitoun, N. Pinna, *Adv. Funct. Mater.* **2007**, *17*, 3159.
[35] I. Bilecka, I. Djerdj, M. Niederberger, *Chem. Commun.* **2008**, 3.
[36] I. Bilecka, P. Elser, M. Niederberger, *ACS Nano* **2009**, *3*, 467.
[37] J. Joo, S. G. Kwon, J. H. Yu, T. Hyeon, *Adv. Mater.* **2005**, *17*, 1873.
[38] H. Du, F. Yuan, S. Huang, J. Li, Y. Zhu, *Chem. Lett.* **2004**, *33*, 770.
[39] I. Djerdj, D. Arcon, Z. Jaglicic, M. Niederberger, *J. Phys. Chem. C* **2007**, *111*, 3614.
[40] N. Pinna, S. Grancharov, P. Beato, P. Bonville, M. Antonietti, M. Niederberger, *Chem. Mater.* **2005**, *17*, 3044.
[41] M. Gotic, S. Music, *Eur. J. Inorg. Chem.* **2008**, 966.
[42] N. Pinna, G. Garnweitner, M. Antonietti, M. Niederberger, *J. Am. Chem. Soc.* **2005**, *127*, 5608.
[43] M. Niederberger, G. Garnweitner, J. Buha, J. Polleux, J. Ba, N. Pinna, *J. Sol-Gel Sci. Techn.* **2006**, *40*, 259.
[44] M. Niederberger, G. Garnweitner, J. Ba, J. Polleux, N. Pinna, *Int. J. Nanotech.* **2007**, *4*, 19.
[45] M. Niederberger, G. Garnweitner, N. Pinna, M. Antonietti, *J. Am. Chem. Soc.* **2004**, *126*, 9120.
[46] M. Niederberger, N. Pinna, J. Polleux, M. Antonietti, *Angew. Chem.* **2004**, *116*, 2320; *Angew. Chem. Int. Ed.* **2004**, *43*, 2270.
[47] L. Z. Zhang, I. Djerdj, M. Cao, M. Antonietti, M. Niederberger, *Adv. Mater.* **2007**, *19*, 2083.
[48] L. Zhang, G. Garnweitner, I. Djerdj, M. Antonietti, M. Niederberger, *Chem. Asian J.* **2008**, *3*, 746.
[49] G. Garnweitner, M. Niederberger, *J. Am. Ceram. Soc.* **2006**, *89*, 1801.
[50] J. Ba, A. Feldhoff, D. Fattakhova Rohlfing, M. Wark, M. Antonietti, M. Niederberger, *Small* **2007**, *3*, 310.
[51] J. Ba, D. Fattakhova Rohlfing, A. Feldhoff, T. Brezesinski, I. Djerdj, M. Wark, M. Niederberger, *Chem. Mater.* **2006**, *18*, 2848.
[52] C. Vázquez-Vázquez, M. Arturo López-Quintela, *J. Solid State Chem.* **2006**, *179*, 3229.
[53] N. Pinna, M. Karmaoui, M.-G. Willinger, *J. Sol-Gel Sci. Techn.* **2010**, DOI: 10.1007/s10971.
[54] N. Pinna, *J. Mater. Chem.* **2007**, *17*, 2769.
[55] C. Sanchez, G. J. D. A. A. Soler-Illia, F. Ribot, T. Lalot, C. R. Mayer, V. Cabuil, *Chem. Mater.* **2001**, *13*, 3061.
[56] N. Pinna, G. Garnweitner, P. Beato, M. Niederberger, M. Antonietti, *Small* **2005**, *1*, 112.
[57] M. Karmaoui, R. A. Sa Ferreira, A. T. Mane, L. D. Carlos, N. Pinna, *Chem. Mater.* **2006**, *18*, 4493.

[58] M. Karmaoui, R. A. Sá Ferreira, L. D. Carlos, N. Pinna, *Mater. Sci. Eng. C* **2007**, *27*, 1368.
[59] M. Karmaoui, M. G. Willinger, L. Mafra, T. Herntrich, N. Pinna, *Nanoscale* **2009**, *1*, 360.
[60] J. Polleux, N. Pinna, M. Antonietti, M. Niederberger, *J. Am. Chem. Soc.* **2005**, *127*, 15595.
[61] J. Polleux, A. Gurlo, N. Barsan, U. Weimar, M. Antonietti, M. Niederberger, *Angew. Chem.* **2006**, *118*, 267; *Angew. Chem., Int. Ed.* **2006**, *45*, 261.
[62] J. Polleux, M. Antonietti, M. Niederberger, *J. Mater. Chem.* **2006**, *16*, 3969.
[63] M.-G. Willinger, G. Clavel, W. Di, N. Pinna, *J. Ind. Eng. Chem.* **2009**, *15*, 883.
[64] I. Bilecka, A. Hintennach, I. Djerdj, P. Novak, M. Niederberger, *J. Mater. Chem.* **2009**, *19*, 5125.
[65] H. Yang, X.-L. Wu, M.-H. Cao, Y.-G. Guo, *J. Phys. Chem. C* **2009**, *113*, 3345.
[66] W. Di, R. A. S. Ferreira, M.-G. Willinger, X. Ren, N. Pinna, *J. Phys. Chem. C* **2010**, *114*, 6290.
[67] G. Garnweitner, J. Hentschel, M. Antonietti, M. Niederberger, *Chem. Mater.* **2005**, *17*, 4594.
[68] J. Matos, J. Laine, J. M. Herrmann, *J. Catal.* **2001**, *200*, 10.
[69] M. R. Hoffmann, S. T. Martin, W. Choi, D. W. Bahnemann, *Chem. Rev.* **1995**, *95*, 69.
[70] N. H. Hong, A. Ruyter, W. Prellier, J. Sakai, *Appl. Phys. Lett.* **2004**, *85*, 6212.
[71] J. D. Bryan, S. A. Santangelo, S. C. Keveren, D. R. Gamelin, *J. Am. Chem. Soc.* **2005**, *127*, 15568.
[72] I. Djerdj, D. Arcon, Z. Jaglicic, M. Niederberger, *J. Solid State Chem.* **2008**, *181*, 1571.
[73] G. D. Yadav, J. J. Nair, *Microporous Mesoporous Mater.* **1999**, *33*, 1.
[74] S. P. S. Badwal, *Solid State Ionics* **2001**, *143*, 39.
[75] D. S. Lee, W. S. Kim, S. H. Choi, J. Kim, H. W. Lee, J. H. Lee, *Solid State Ionics* **2005**, *176*, 33.
[76] P. Li, I.-W. Chen, J. E. Penner-Hahn, *J. Am. Ceram. Soc.* **1994**, *77*, 118.
[77] Y. Xie, *J. Am. Ceram. Soc.* **1999**, *82*, 768.
[78] R. C. Garvie, *J. Phys. Chem.* **1978**, *82*, 218.
[79] T. Ninjbadgar, G. Garnweitner, A. Börger, L. M. Goldenberg, O. Sakhno, J. Stumpe, *Adv. Funct. Mater.* **2009**, *19*, 1819.
[80] G. Clavel, M.-G. Willinger, D. Zitoun, N. Pinna, *Eur. J. Inorg. Chem.* **2008**, *2008*, 863.
[81] A. Pucci, G. Clavel, M.-G. Willinger, D. Zitoun, N. Pinna, *J. Phys. Chem. C* **2009**, *113*, 12048.
[82] P. Ghosh, A. Patra, *Langmuir* **2006**, *22*, 6321.
[83] A. Mondal, S. Ram, *J. Am. Ceram. Soc.* **2008**, *91*, 329.
[84] P. Ghosh, K. R. Priolkar, A. Patra, *J. Phys. Chem. C* **2006**, *111*, 571.
[85] Z. W. Quan, L. S. Wang, J. Lin, *Mater. Res. Bull.* **2005**, *40*, 810.
[86] H. Arashi, *Physica Status Solidi A* **1972**, *10*, 107.
[87] J. Dexpert-Ghys, M. Faucher, P. Caro, *J. Solid State Chem.* **1984**, *54*, 179.
[88] I. Bilecka, M. Niederberger, *Nanoscale* **2010**, DOI: 10.1039/b9nr00377k.